Flexible Tactile-Sensing Gripper Design and Excessive Force Protection Function for Endovascular Surgery Robots

Chuqiao Lyu , Shuxiang Guo , *Fellow, IEEE*, Yonggan Yan , Yongxin Zhang , Yongwei Zhang , Pengfei Yang , and Jianmin Liu

Abstract—Research on endovascular surgery robots (ESR) is continuously developing, because ESR can protect surgeons from radiation exposure. For designing an ESR manipulator, the main challenge is controlling the soft surgical tools and measuring the endovascular stress simultaneously. In this letter, a flexible tactile-sensing gripper (FTG) is designed to realize the stable grasping of the surgical catheter and the tactile sensing of catheter force. Firstly, a catheter grasping model was constructed, and the factors affecting the force measurement were quantitatively analyzed. Secondly, the simulation experiments based on FTG models with three different sizes were implemented. When the catheter force was too large, shrinking the grasping distance of FTG can avoid the surgical risk. This method protected the surgeon's behavior and controlled the catheter force at the same time, which was called excessive force protection function (EFPF). Thirdly, based on simulation results, we made a FTG prototype which meet the surgical requirements and integrated it into an ESR manipulator. This manipulator could measure the catheter forces by detecting the coordinate change of marking points on FTG surface. The calibrated FTG prototype got average and maximum errors of force sensing approximately 37 mN and 223 mN, respectively. Finally, the proposed EFPF is evaluated. In the experiment of carotid artery catheterization, EFPF controlled the catheter force within 393 mN, which was far less than the control group's 1351 mN.

Index Terms—Medical robots and systems, soft sensors and actuators, force and tactile sensing.

I. INTRODUCTION

ENDOVASCULAR surgery is an effective method for treating cardiovascular and cerebrovascular diseases such as aneurysms and strokes. However, surgeons who performing endovascular surgery may get the extended risks, such as physical fatigue and radiation exposure [1]. Therefore, the endovascular surgery robot (ESR) systems, such as Corpath GRX [2] and Sensei X [3], have been developed to assist surgeons in performing operations remotely. The teleoperated ESR system consists of two components: the operator side and the gripper side. The operator side captures the surgeon's actions, while the gripper side grabs the surgical instruments (e.g. catheters and guidewires) and reproduces the surgeon's actions on the operating table.

Due to the rigid grasping of ESR manipulators, the surface of catheter may be damaged, which will affect the insertion of the guidewire. In severe cases, a damaged catheter fragment may enter the human body and cause thrombosis [4]. Furthermore, the force sensing ability of ESR manipulators is equally important. An ESR manipulators used tactile feedback can improve the surgical safety. Because the excessive catheter forces may damage or even punch the blood vessel walls [5]. To sum up, it is very important for ESR manipulators to grasp the catheter flexibly and measure the force at the same time.

For solving the above problems, several studies have focused on the suitable gripper structures. For instance, Kundrat et al. [6] proposed a pneumatic motor to realize the simultaneous grasping adaptation of catheters and guidewires. Choi et al. [7] designed side-by-side rolling cylinders to realize the forward movement of catheters. Their robot had the advantage of volume reduction and simultaneous operation with multiple instruments. Considering the force-sensing functions, Bao et al. [5] designed a four-claw structure to realize grasping action in a narrow space through a wedge-shaped slider. The structure acquired the accurate control and measurement of forces, but their method required the special grippers to adapt to different sizes of catheters. Jin et al. [8] used springs as the grasping support. The load cell was placed next to the spring to measure the force, and a dynamic torque sensor was used to measure the torque. Although the spring could adapt to different catheter sizes, the grasping force could not be controlled in their robot. Furthermore, Yan et al. [9] measured the force by spring deformation and controlled the grasping force during the operation. There were also many ESR systems with well-designed robot structures are found in recent studies [10], [11].

The research on rigid grippers of ESR is mature, but their flexibility is inferior to human fingers. The flexible fingers of surgeons can accurately control the catheter force and avoid the surgical risks, as shown in Fig. 1(a). Clinically, soft materials are
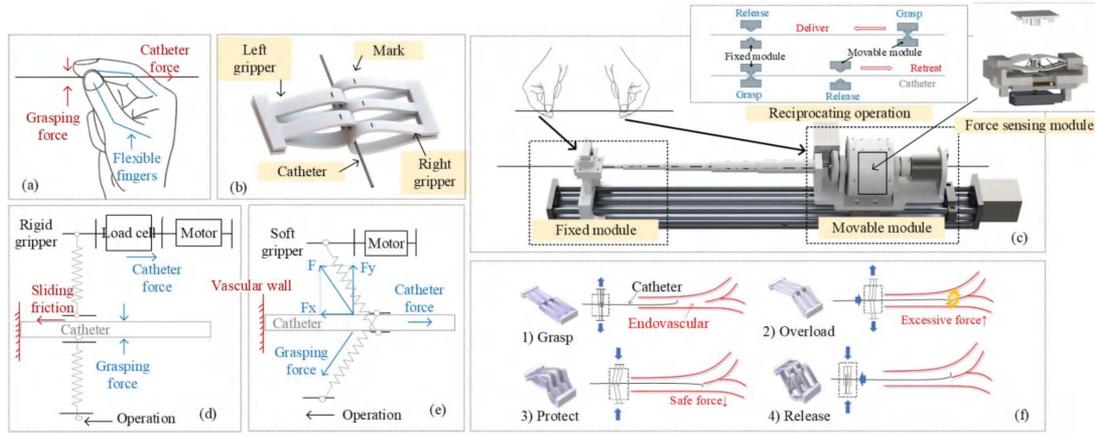
Fig. 1. Main contributions of this study. (a) Human fingers. (b) Flexible tactile-sensing gripper (FTG). (c) Manipulator. (d) Rigid gripper. (e) Soft gripper. (f) Excessive force protection function (EFGF).

widely used in surgery, such as catheters [12] and stents [13]. The grippers made with soft materials have better adaptability to the supported objects. On the one hand, they can stably grab thin objects without damaging its surface [14]. On the other hand, some studies show that the soft gripper can measure the force [15] and make skillful movements [16] like human fingers. However, according to ours investigation, there is still a lack of research on making grippers or manipulators with soft materials in ESR.

This study presents a flexible tactile-sensing gripper (FTG) which grabs surgical catheters through a soft, parallel, and lasso-like structure, as shown in Fig. 1(b). The proposed soft gripper has several advantages over the rigid gripper. The grasping principles of two kinds of grippers are drawn in the Fig. 1(d), (e). Firstly, the proposed soft gripper measures the catheter force through visual positioning, thus avoiding the influence of motor vibration on the load cell. Secondly, as shown in Fig. 1(e), the soft grippers have the ability to deform in the direction of catheter insertion. When the catheter is blocked in blood vessels, the deformation of soft grippers can bring a buffer zone, which avoid the relative sliding on the grasping point and reduces the risks of surgery. Thirdly, by changing the grasping distance, FTG can control the catheter force by adjusting the elastic deformation. This function is exploited in this study to avoid the surgical risks, which is called excessive force protection function (EFPF) and shown in Fig. 1(f). Finally, a manipulator which meets the surgical requirements is designed and shown in Fig. 1(c). In this manipulator, the reciprocating operation is realized by the cooperation of two grippers.

The gripper design details, including structure and kinematics, hyperelastic model and grasping model, are described in Section II. The simulation model is introduced in Section III. Section IV demonstrates the integration of manipulator. Section V carries out two evaluation experiments. Last, the conclusions are presented in Section VI.

II. GRIPPER

There is a strict limit for catheter force in endovascular surgery. Firstly, the required range of catheter force varies across different endovascular locations. According to some studies [10], for percutaneous coronary intervention (PCI) and
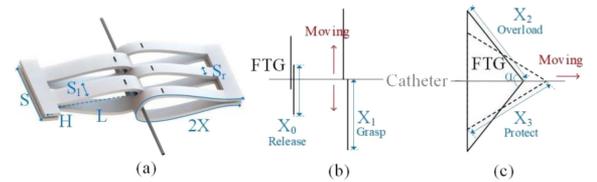

Fig. 2. Structure and kinematics of FTG. (a) Gripper structure. (b) Release and grasp. (c) Overload and protect.

neuro-vascular intervention (NVI), there is a risk of vascular injury if the catheter force exceeds 0.5 N. However, in percutaneous peripheral intervention (PPI), the risk force threshold of up to 2 N. Secondly, differences in force control levels during surgery exist between experienced and inexperienced surgeons. In PCI surgery, several studies [17] have reported that experienced surgeons can limit the maximum catheter force to no more than 0.54 N, but the inexperienced surgeons can only control it within 1.75 N. To sum up, a suitable gripper needs to be able to measure the catheter force over 2 N, and achieve accurate control of the catheter force within 0.5 N. Therefore, the quantitative analysis of FTG grasping force model is very important.

A. Structure and Kinematics

The structure of FTG is shown in Fig 2(a). The shapes of the grippers on the left and right sides are different. The left gripper has two lassoes (width S_l) and the right has three lassoes (width S_r). The whole width S on both sides is equal, so $S/2 = 2S_l = 3S_r$. FTG is made by a piece of natural rubber with a thickness H. Then it is folded into the manipulator (See Fig. 9(b) for details). L is the distance between the catheter and the moving part of grippers, which is regarded as the grasping distance. The manipulator designed in this study can change L by controlling a linear motor (See Fig. 8(b) for details). $2X$ in Fig 2(a) represents the overall length of the unfolded FTG. Here, assuming FTG and the catheter are straight lines, then the deformation of each lasso can be represented by a variable X and shown in Fig. 2(b), (c). The variable X can be divided into four states: 1) Release: In Fig. 2(b), when the gripper is released, $X = X_0$. 2) Grasp: When

the gripper is tightened, $X = X_1$. 3) Overload: In Fig. 2(c), when the catheter force is applied to the FTG, $X = X_2$. At this time, FTG forms a solid triangle and has an angle α. 4) Protect: If there is a surgical risk (e.g. catheter force exceeds 0.5 N), manipulator will shrink the grasping distance L. At this time, α will decrease, and FTG forms a dotted triangle in Fig. 2(c), $X = X_3$.

B. Hyperelastic Model

FTG's grasping force F is related to the stretch ratio $\lambda = X_i/X_0 (i = 1,2,3)$. For a hyperelastic material such as natural rubber, the function $F(\lambda)$ is nonlinear. We use the strain-energy density function W to express the stress-strain relationship. In general, W can be expressed as

$$W = f(I_1, I_2, I_3), \tag{1}$$

where I_i $(i = 1, 2, 3)$ represents the strain invariant. For any given coordinate system, the value of I_i remains the same. Assuming the natural rubber is incompressible, $I_3 = 1$. Therefore, W based on two parameters Mooney–Rivlin model can be expressed as

$$W = C_1(I_1 - 3) + C_2(I_2 - 3), \tag{2}$$

where C_1 and C_2 are material parameters. We refer to this paper [18] and choose Mooney-Rivlin model instead of Ogden model. Mooney-Rivlin model can be better applied to the small deformations of rubber materials (elastic deformation and λ within 200%), but Ogden model is more suitable for the large deformations (plastic deformation). If plastic deformation occurs, the catheter force cannot be calibrated. In this study, the maximum stretch ratio $\lambda_{\max} = X_{\max}/X_0$, where $X_0 = 30$ mm and $X_{\max} = \sqrt{36^2 + 20^2} \approx 41$ mm (as deduced from Fig. 10(b)). Therefore, $\lambda_{\max} \approx 132\%$, and Mooney-Rivlin model can fit it well. Next, the relationship between the Cauchy stress σ_i and stretch ratio λ_i is

$$\sigma_i = 2\left(\lambda_i^2 \frac{\partial W}{\partial I_1} + \frac{1}{\lambda_i^2} \frac{\partial W}{\partial I_2}\right) + p, \tag{3}$$

$$\lambda_i = \frac{X_i}{X_0}, \tag{4}$$

where p is hydrostatic pressure. X_0 is the initial length, and X_i is the deformation length in the ith direction. When FTG is deformed, the difference of stress σ_i in the three directions is expressed as

$$\sigma_1 - \sigma_2 = 2(\lambda_1^2 - \lambda_2^2)\left(\frac{\partial W}{\partial I_1} + \lambda_3^2 \frac{\partial W}{\partial I_2}\right),$$

$$\sigma_2 - \sigma_3 = 2(\lambda_2^2 - \lambda_3^2)\left(\frac{\partial W}{\partial I_1} + \lambda_1^2 \frac{\partial W}{\partial I_2}\right),$$

$$\sigma_3 - \sigma_1 = 2(\lambda_3^2 - \lambda_1^2)\left(\frac{\partial W}{\partial I_1} + \lambda_2^2 \frac{\partial W}{\partial I_2}\right). \tag{5}$$

For the equibiaxial tensile model, $\sigma_3 = 0$, $\lambda_1 = \lambda_2 = \lambda$, and $\lambda_3 = \lambda$. Hence, (5) is simplified to

$$\sigma_1 = \sigma_2 = 2(\lambda^2 - \lambda^{-4})(C_1 + \lambda^2 C_2). \tag{6}$$

The second Piola-Kirchhoff stress p_s can represent the normal stress in the initial state. Because $\sigma = \lambda \times p_s$,

$$p_s = 2(\lambda - \lambda^{-5})(C_1 + \lambda^2 C_2), \tag{7}$$

TABLE I
MOONEY-RIVLIN PARAMETERS

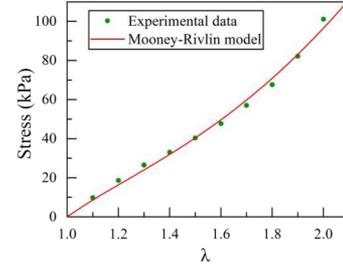| Parameter	Value (kpa)	Parameter	Value (kpa)
C_1	2.247	C_2	5.567

Fig. 3. Experimental data is generated by performing an equibiaxial tensile test, and the Mooney–Rivlin model fits the data.
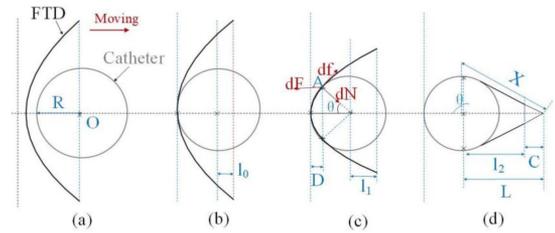

Fig. 4. Four states of grasping model. (a) Release. (b) Contact. (c) Adapt. (d) Grasp.

where C_1 and C_2 are the constitutive parameters of rubber material expressed by the Mooney–Rivlin model. A rectangular sample (length 30 mm, width 30 mm, thickness 1.5 mm) based on the rubber material used for the equibiaxial tensile test, is used to obtain these parameters. The sample is stretched ten times at different stretching ratios and recorded the values of stress. The least square method is used to obtain C_1 and C_2 in (7). Table I lists the Mooney–Rivlin parameters obtained using the curve fit, and Fig. 3 shows the tensile data and function.

C. Grasping Model

The connection between FTG and catheter has been assumed as a point in Fig. 2(b). In this part, a general grasping model is demonstrated. This model is available for catheters of different sizes. Here we analyze a catheter's cross-section, as shown in Fig. 4. According to the change of grasping distance L, There are also two states of Contact and Adapt between Release and Grasp.

1) Release: When the distance L is 0, a fixed distance is insufficient to connect the catheter with FTG.

2) Contact: When $L = L_0$, FTG touches the catheter and has no deformation.

3) Adapt: When L is increased to L_1, FTG will be semi-wrapped on the catheter's surface. This deformation varies according to the radius of the catheter. Let θ be the angle between the horizontal direction and farthest contact point. If an infinitesimal $d\theta$ is selected for stress analysis, assuming that the friction factor μ is constant, then the normal force dN and
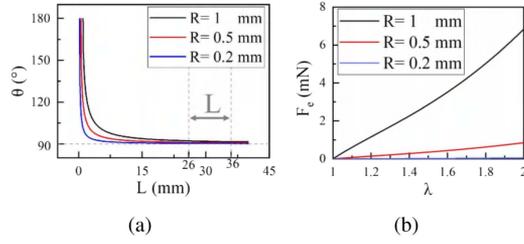
Fig. 5. Relationship between the angle θ, the grasping force F and the grasping distance L. (a) Illustration of (12). (b) Grasping force error caused by the change of θ.

FTGs	H (mm)	X (mm)	S (mm)	S_l (mm)	S_r (mm)
A	1.5	30	24	6	4
B	1.5	30	18	4.5	3
C	1.5	30	12	3	2

friction df acting on the catheter surface can be expressed as

$$dN = 2p_s RS d\theta \tag{8}$$

$$df = \mu dN, \tag{9}$$

where p_s is the applied contact pressure by FTG, which is equivalent to p_s in (7). S is the FTG width, and R is the catheter radius. According to the force analysis, the grasping force dF is the total force of dN and df in the horizontal direction.

$$dF = dN \cos(\theta) + df \sin(\theta). \tag{10}$$

Integrating angle θ, the integral of F is expressed as

$$
\begin{aligned}
F &= p_s RS \int_{-\theta}^{\theta} [\cos(\theta) + \mu \sin(\theta)] \, d\theta \\
&= 2p_s RS \sin(\theta)
\end{aligned}
\tag{11}
$$

According to (11), due to the variable θ, the grasping force F is nonlinear with its width S.

4) Grasp: When L reaches the maximum, FTG grabs the catheter and performs the surgery. At this time, angle θ can be expressed as

$$\cos(\theta) = -\frac{R}{L}, \tag{12}$$

Therefore, the relationship between L and θ is plotted in Fig. 5(a). Ideally, keeping the angle θ at 90 degrees will not interfere with the grasping force. But considering the different sizes of catheters, the real contact area between FTG and catheter is a cylindrical surface. When the FTG moves (e.g. Fig. 2(c)), the value of θ is difficult to calculate accurately. An appropriate method is to minimize the influence from θ. In this study, we have set the actual range of L from 26 mm to 36 mm. According to Fig. 5(a), θ will change slightly in this range. The grasping force error accumulates with the increase of catheter radius. Combining the (11), (12) and (7), the grasping force error F_e (caused by L) can be calculated.

$$F_e = F(L=36) - F(L=26) \tag{13}$$

The relationship between F_e and λ is shown in Fig. 5(b). Here, the width of FTG is regarded as a basic unit ($S = 1$ mm). With the increase of the radius of catheters, the contact surface between FTG and the catheter has greater influence on the measurement of grasping force. According to (11), it will not be affected in the process of Grasp state and Relase state (Fig. 2(b)). However, when the FTG has triangular deformation (Fig. 2(c)), it will

lead to a slight imbalance in the grasping forces of both sides of FTG, thus affecting the measurement accuracy of the catheter force. In order to explore the performance of FTG. Three FTGs with different width S are designed, and their sizes are shown in Table II.

III. SIMULATION

A. Simulation Parameters and Steps

According to Table II, three FTG models are made. They grab the catheters which have two sizes ($R = 0.5$ mm, 1 mm). Each lasso of FTG has an end part (length 4 mm) which is movable. In the real environment, due to the change of contact surface between FTG and catheters, the friction coefficient μ between catheter and FTG always changes. Here, we ignore the sliding friction, and set μ to a constant value of 0.95. Under this condition, three quasi-static steps are simulated and implemented.

1) Step 1: In Fig. 6(a), the catheter is fixed, and the grippers are stretched along the X direction. The left and right grippers of FTG are stretched to $x = -10$ mm and 10 mm (L is changed from ±26 mm to ±36 mm, respectively). This step realizes the grasping function of FTG.

2) Step 2: The grippers are fixed, and the catheter is moved along the Y direction. As shown in Fig. 6(d), the catheter is moved first from $y = 10$ mm to -10 mm, then from $y = -10$ mm to 10 mm. This process simulates the FTG strain when the catheter force is applied during operation.

3) Step 3: The catheter is fixed again at $y = 10$ mm, and the grippers are shrunk to $x = -4$ mm and 4 mm (L is changed from ±36 mm to ±30 mm, respectively), as shown in Fig. 6(g). This process simulates the protection function when the catheter receives excessive forces.

B. Result Analysis

The X-axis force is measured by the pressure of the right side FTG against the catheter surface. The Y-axis force is measured by the friction of the both sides FTG against the catheter surface. Without considering the sliding friction, we assume that the Y-axis force and the catheter force are interactive forces. Fig. 6(b), (c) are obtained according to Step 1. During the states from Relased to Grasp, the X-axis force increases nonlinearly. At this time, the Y-axis force is only approximately 1 mN. Fig. 6(e), (f) record the simulation results of Step 2. The results in Fig. 6(f) show that increasing the FTG width S can increase the measurement range of catheter forces. The catheter force ranges are obtained about ±1.60 N for FTG A, about ±1.21 N for FTG B, and about ±0.81 N for FTG C. However, the force results differ in different catheters' sizes, making separate calibration necessary. The X-axis and Y-axis forces present a linear release trend in Step 3 (Fig. 6(h), (i)). When reducing L, both X-axis force and Y-axis force will decrease, which means that it is feasible to avoid excessive force by shrinking FTG.

(a)

(b)

(c)

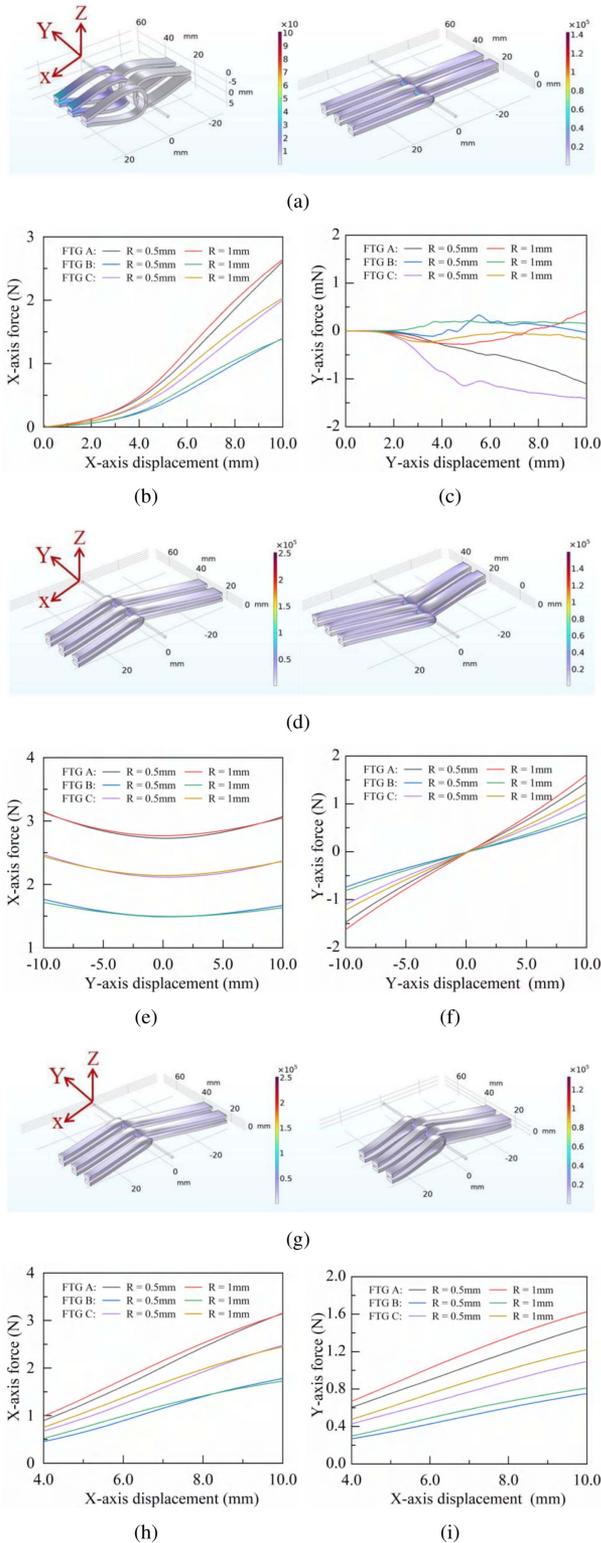(d)

(e)

(f)

(g)

(h)

(i)

Fig. 6. Simulation steps of FTG. (a) In Step 1, the catheter is stationary, and FTG is stretching (X-axis displacement); (d) In Step 2, the FTG is stationary, and the catheter makes reciprocating motions (Y-axis displacement); (g) In Step 3, the catheter is stationary again, and the FTG contracts (X-axis displacement); (b), (e), (h) represents the grasping force (X-axis force) from the right side of FTG; (c), (f), (i) represents the catheter force (Y-axis force) from the both right and left sides of FTG. Where (c), (b) corresponds to Step 1; (e), (f) corresponds to Step 2 and (h), (i) corresponds to Step 3.
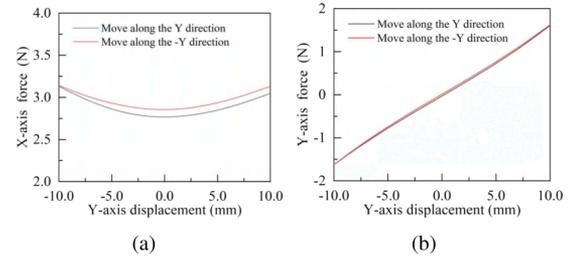

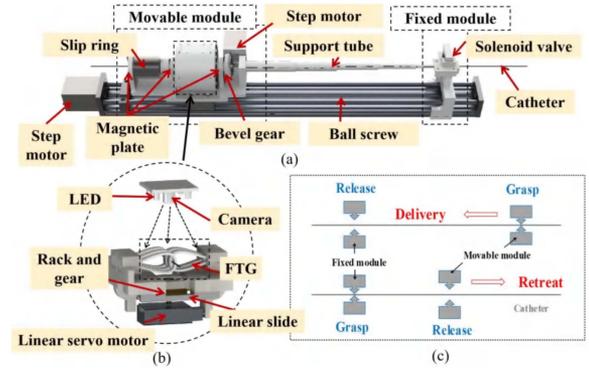Fig. 7. Restoring force curve in Step 2. (a) X-axis force; (b) Y-axis force.

Fig. 8. Manipulator integration. (a) Manipulator. (b) Vision-based Force Measurement. (c) Reciprocating operation.

Due to the influence of angle θ in (11), there is a asymmetry surface between the catheter and the two sides of FTG. When the loads (catheter forces) in different directions are applied, the friction effects between FTG and catheter are not equal. In Step 2, if the directions of FTG deformation along the Y-axis are different, the catheter force changes are also different. This phenomenon is known as the restoring force curve. For example, when the FTG ($S = 24$ mm) grabs a catheter ($R = 1$ mm), the restoring force curve obtained from simulation results is shown in Fig. 7(a), (b). The maximum force errors caused by different directions of FTG deformation are about 88 mN in Fig. 7(a) and 18 mN in Fig. 7(b), respectively. Therefore, in order to reduce the measurement error of catheter forces, it is necessary to calibrate catheter forces from two directions (Delivery and Retreat, see Fig. 10(b) for details).

IV. MANIPULATOR

A. Reciprocating Operation

The proposed manipulator motion contains three degrees of freedom (grasping, translating, and rotating), which are realized by the two module, as shown in Fig. 8(a). Both the fixed module and the movable module are placed on a linear rail. The moving gripper is fixed on a magnetic plate. The catheter can be quickly removed with the movable module by removing the magnetic plate (See Fig. 9(a) for details). Next, when the fixed module releases the catheter, the movable module will grab the catheter and perform the delivery action. When the fixed module grabs the catheter, the movable module will release the catheter and perform the retract action. This reciprocating operation makes
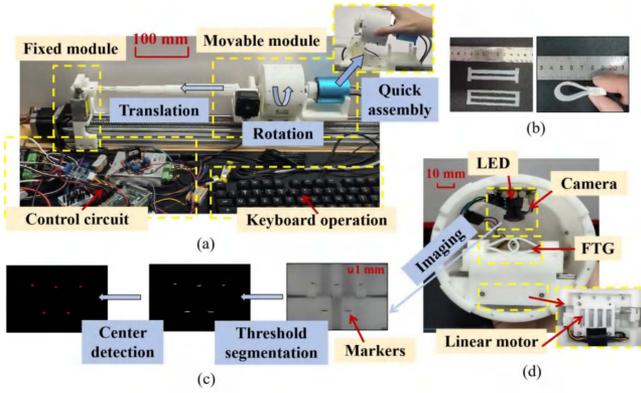
Fig. 9. Prototype. (a) Manipulator system. (b) Unfold and fold states of FTG. (c) Marked points. (d) Movable module.

the manipulator control the arbitrary length of the catheter, as shown in Fig. 8(c).

B. Vision-Based Force Measurement

The FTG is deployed inside the movable module and driven by a linear motor at the bottom, as shown in Fig. 8(b). Two parallel racks mesh with a gear that drives each side of FTG to move the same distance. A camera captures the artificial marked points on FTG surface. When the catheter force is applied, FTG will be deformed. The catheter force can be accurately measured by calculating the points' displacements. Therefore, the relationship between coordinate values P_i and catheter force F can be expressed using function g as

$$F = g(\bar{P}), \quad \bar{P} = \frac{\sum_{i=1}^{5} P_i}{5}. \tag{14}$$

In this study, FTG is marked with five points. $\bar{P}$ is obtained by calculating the abscissa value of the points. Considering the restoring force curve (mentioned in Section III-B), function g need be split in the directions of catheter forces.

$$F = \begin{cases} g_1(\bar{P}), & \Delta P > 0. \\ g_2(\bar{P}), & \Delta P < 0. \end{cases} \tag{15}$$

where ΔP represents the changes of abscissa values in a continuous time. Compared with the manipulators carried high-precision force sensors [5], [8], [9], the vision-based force sensing manipulator reduces the manufacturing costs. Therefore, the special FTG can be prepared for each catheter before operation, which realizes the rapid replacement of catheters during the surgery.

C. Prototype

The prototype of manipulator is established and shown in Fig. 9(a). The control system uses Arduino as the lower computer and PC as the upper computer, which communicate through the 485 protocol. The electromagnet (ZYE1-1253, peak voltage 12 V, stroke 10 mm, manufactured by CNZYEM, China) on the linear rail (EBX-1605, stroke 600 mm, manufactured by OUBANG, China) is controlled by an L298 N module. The stepper motor (STM5756B, manufactured by NiMotion, China) driving the translation of catheter keeps a constant speed of

3.125 mm/s, and the stepper motor (STM4234B, manufactured by NiMotion, China) driving the rotation of catheter keeps a constant speed of 3.925 rd/s. The grasping distance L of the manipulator is controlled by a linear motor (LAS16, maximum speed 26 mm/s, self-locking force exceeds 150 N, manufactured by INSPIRE-ROBOTS, China). By removing the magnetic plate, the movable module and the catheter can be quickly removed and replaced, as shown in the upper right corner of Fig. 9(a). Compared with robots with force sensors, FTG reduces the manufacturing cost of robots. Surgeons can prepare multiple sterilized movable modules before the surgery and replace them after use. This not only ensures the robot sterility, but also improves the efficiency of catheters/guidewires replacement.

The prototype of FTG is shown in Fig. 9(b). According to the simulation results and surgical requirements, we made a FTG prototype according to the size of FTG A in Table II and integrated it into the robot, as shown in Fig. 9(b), (d). The marked points are captured by a camera (customized, resolution 800×600, viewing angle $170°$, frequency 60 Hz) and processed using the OpenCV software, as shown in Fig. 9(c). A white baffle is placed under the FTG in Fig. 9(d), one of its functions is as a white background to improve the recognition rate of points, and the other is to support the relaxed FTG. The control frequency of the whole system is about 50 Hz. Note that the frequency of catheter force in clinical practice can be defined by a standard range (30 Hz–60 Hz [10]) that are perceptible by the human hand. When the force output frequency falls below 30 Hz, the force information may need to be compensated using algorithms such as kalman filter [19]. In this study, the camera sends the FTG image to PC, and PC calculates the force according to (15) in real time. Therefore, the force output frequency is affected by the speed of image processing. Considering the calculation time of OpenCV algorithms, the catheter force output frequency is stably controlled at 30 Hz.

D. Calibration

The platfrom of calibration experiment is designed and shown in Fig. 10(a). The FTG is connected to a load cell (SBT673, measuring range ± 20 N, composite error $\pm 0.1\%$, manufactured by SIMBATOUCH, China) by a metal rod ($R = 1$ mm). When FTG grabs the rod, FTG will be deformed but the rigid rod will not, and the force will be captured by the load cell. Next, we repeat the operation of Section III.A.2. The time of operation lasts about 15 s. Note that the marking points on the FTG surface can not exceed the camera's field of view. Finally, the coordinates (P_i) and load cell force (F) are recorded, and (15) is calculated by the three-section polynomial fitting.

Fig. 10(b) shows the relationship between the average coordinates $\bar{P}$ and load cell force F at grasping distance $L = 36$ mm. Compared with the simulation process (Fig. 7(b)), FTG prototype has a greater amount of deformation. Therefore, the force measurement range of the FTG prototype is from -4.46 N to 3.74 N. According to the analysis of Section II, the proposed manipulator can meet the surgical requirements. When L changes, the calibration results are recorded and shown in Fig. 11(a). The errors considering restoring force curve ((15)) are about 37 mN (Avg.) and 223 mN (Max.). Compared with the results without restoring force curve ((14)), average error and maximum error are decreased by 48.6% (73 mN) and 5.6% (237 mN), respectively. In order to verify the dynamic response specification of FTG, we compare FTG with the load cell.
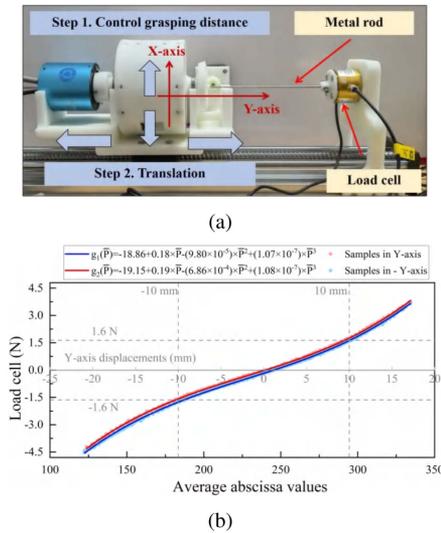
Fig. 10. Calibration experiment. (a) Experiment platform; (b) Calibration results.
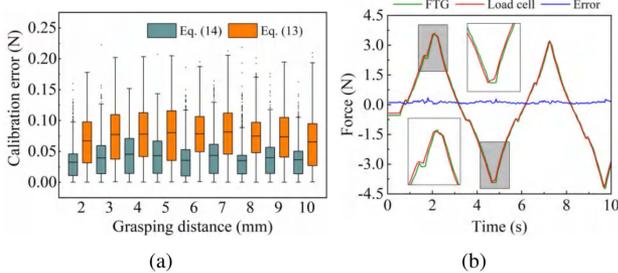

Fig. 12. Excessive force protection experiment. (a) $\Delta L = 0.2$ mm. (b) $\Delta L = 0.4$ mm. (c) $\Delta L = 0.6$ mm. (d) $\Delta L = 0.8$ mm.

Fig. 11. Error analysis. (a) Force errors when L changes. (b) Real-time following errors.

Firstly, the calibrated manipulator is controlled to reciprocate on the platform (Fig. 10(a)) at a period of 5 s. Secondly, a 10 s data is intercepted, and recorded in Fig. 11(b). The load cell's output frequency is down-sampled to 30 Hz and matches FTG. Finally, the calibrated FTG exhibits good follow-up with the load cell, which has an average error of approximately 106 mN in real-time, as shown in Fig. 11(b).

V. EXPERIMENT AND EVALUATION

A. Excessive Force Protection Experiment

1) Method: As mentioned above, the excessive force protection function (EFPF) is important for limiting the catheter force and avoiding surgical risks, which is realized by changing the grasping distance of FTG. Objectively, EFPF will not affect the surgeon's behavior. However, due to the memory characteristics of soft mterials, the grasping force will deviate when the grasping distance changes. In this experiment, the apparatus is the same as Fig. 10(a). We operate the robot to reciprocate under a variable grasping distance. For EFPF, the 400 mN safe catheter force value is preset. Therefore, the manipulator will actively shrink the FTG when the catheter force exceeds 0.4 N. The shrinking action is stepwise. When a excessive force is applied, the linear
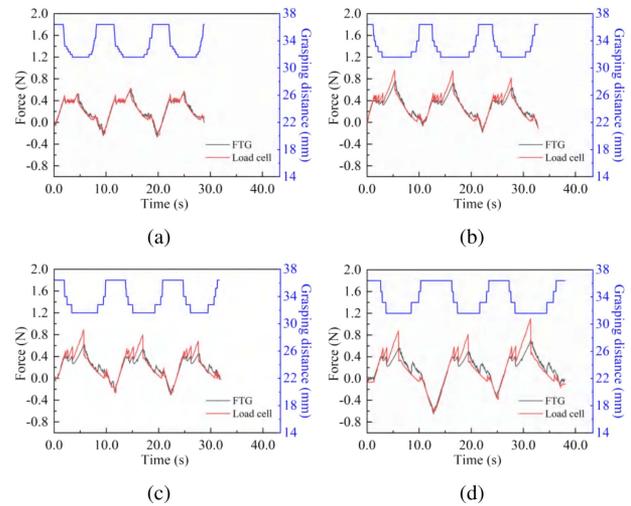
motor will control FTG (at a speed of 26 mm/s) to actively contract by ΔL. The experimental results are shown in Fig. 12.

2) Result: In Fig. 12, four attempts with EFPF are realized, which $\Delta L = 0.2$ mm, 0.4 mm, 0.6 mm and 0.8 mm, respectively. In Fig. 12(a), the black line are the force measured by FTG, and the red line are the force measured by load cell. The results show that when EFPF is triggered, the excessive force will be quickly reduced. Here we set the minimum value of L to 32 mm. If $L <$ 32 mm, the catheter will be released directly by the manipulator. Another results indicate that increasing the continuity of EFPF can reduce the force errors between FTG and load cell. When $\Delta h_m = 0.8$ mm in Fig. 12(d), the maximum force error can reach 398 mN. When $\Delta h_m = 0.2$ mm in Fig. 12(a), the maximum error is 176 mN. Although the error is large, FTG maintains high force measurement accuracy when distance L is constant. In this experiment, the average error Fig. 12(a) is only 30 mN.

B. Carotid Artery Catheterization Experiment

1) Method: A carotid artery catheterization experiment is conducted in the Endo Vascular evaluator (EVE). EVE is a mature commercial equipment and simulates the real blood vessel properties. It has also been used in our previous research [20]. Therefore, it is reasonable to use EVE as ESR's experimental platform. In this study, we use red saline instead of blood. Two comparative experiments were designed, one is operating the manipulator directly and the other is operating the manipulator with EFPF. In EFPF, the ΔL is set to 0.2 mm.

An operator with no surgical experience is invited for the experiment. The operator spent 10 min to familiarize with the manipulator, but was not informed with the surgical path. The catheter movements is observed through an external camera, which simulates X-ray conditions. The FTG is observed through the internal camera. If the FTG shrinks due to EFPF, the operator can find out from the screen and adjust the operation to avoid excessive force in time. During this experiment, the catheter passes through the complex and multi-channel aortic arch and until into carotid artery, as shown in Fig. 13(b). Finally, we recorded the operations and catheter forces, as shown in Fig. 14.
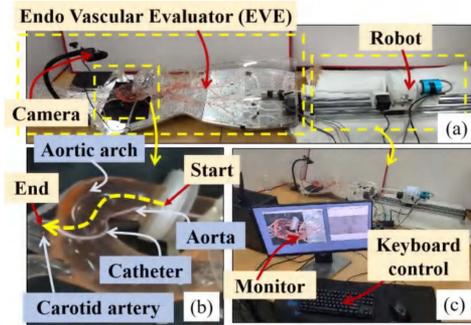
Fig. 13. Carotid artery catheterization experiment. (a) Experiment platform. (b) Carotid artery catheterization. (c) Control system.
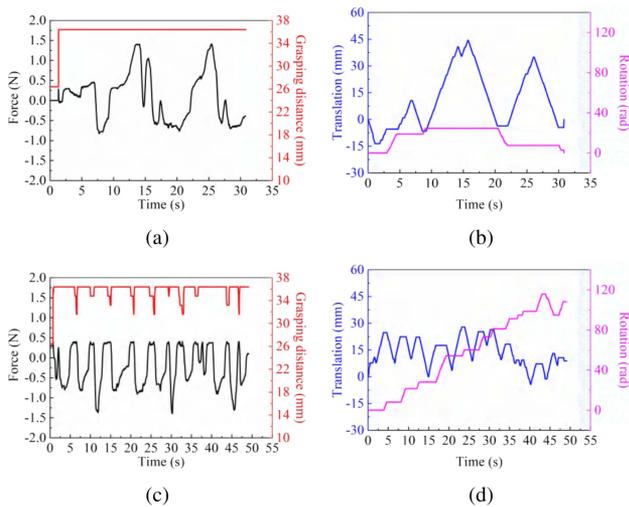

Fig. 14. Results of the carotid artery catheterization experiment. (a) Force curve without EFPF. (b) Displacement curve without EFPF. (c) Force curve with EFPF. (d) Displacement curve with EFPF.

2) Result: Without the EFPF, the operator needs a maximum catheter force of 1351 mN to complete catheterization. In contrast, the EFPF can control the catheter force within 393 mN, which significantly reduces the surgical risks. However, the operating time is also increased from 30 s to 49 s. It is challenging to insert the catheter with a small force range, so the actions of rotating the catheter under the influence of EFPF is increased.

VI. CONCLUSION

In this study, a flexible tactile-sensing gripper (FTG) for endovascular surgery robot was designed. The simulation model based on Mooney–Rivlin was developed to evaluate FTG characteristics. The prototype of FTG could measure catheter force exceeding 3.7 N and control the average error within 37 mN, which meet the requirements of surgical operation. An excessive force protection function (EFPF) was proposed. In carotid artery catheterization experiment, the EFPF-based manipulator could control the catheter forces within 393 mN, which significantly improved the safety of operation. However, the more accurate

range of catheter forces needs to be determined by combining expert experience and clinical practice. Torque detection of catheters is also very important for surgical safety and will be the focus of our future research. Furthermore, because FTG reduces the cost of ESR, this is significant for ESR using in remote areas which lack surgical conditions or budgets.

REFERENCES

[1] S. M. R. Biso and M. I. Vidovich, "Radiation protection in the cardiac catheterization laboratory," *J. Thoracic Dis.*, vol. 12, no. 4, pp. 1648–1655, 2020.

[2] C. Beaman, H. Saber, and S. Tateshima, "A technical guide to robotic catheter angiography with the Corindus CorPath GRX system," *J. NeuroInterventional Surg.*, vol. 14, no. 12, 2022, Art. no. 1284.

[3] F. Cepolina and R. P. Razzoli, "An introductory review of robotically assisted surgical systems," *Int. J. Med. Robot. Comput. Assist. Surg.*, vol. 18, no. 4, 2022, Art. no. e2409.

[4] A. A. Lukito, R. Pranata, I. Huang, A. Thengker, and M. Wirawan, "Fracture of the port catheter and migration into the coronary sinus: Case report and brief review of the literature," *Clin. Med. Insights: Case Rep.*, vol. 12, 2019, doi: 1179547619832282.

[5] X. Bao et al., "Multilevel operation strategy of a vascular interventional robot system for surgical safety in teleoperation," *IEEE Trans. Robot.*, vol. 38, no. 4, pp. 2238–2250, Aug. 2022.

[6] D. Kundrat et al., "An MR-Safe endovascular robotic platform: Design, control, and ex-vivo evaluation," *IEEE Trans. Biomed. Eng.*, vol. 68, no. 10, pp. 3110–3121, Oct. 2021.

[7] J. Choi, S. Park, Y.-H. Kim, Y. Moon, and J. Choi, "A vascular intervention assist device using bi-motional roller cartridge structure and clinical evaluation," *Biosensors*, vol. 11, no. 9, 2021, Art. no. 329.

[8] X. Jin, S. Guo, J. Guo, P. Shi, T. Tamiya, and H. Hirata, "Development of a tactile sensing robot-assisted system for vascular interventional surgery," *IEEE Sensors J.*, vol. 21, no. 10, pp. 12284–12294, May 2021.

[9] Y. Yan et al., "Machine learning-based surgical state perception and collaborative control for a vascular interventional robot," *IEEE Sensors J.*, vol. 22, no. 7, pp. 7106–7118, Apr. 2022.

[10] A. Hooshiar, S. Najarian, and J. Dargahi, "Haptic telerobotic cardiovascular intervention: A review of approaches, methods, and future perspectives," *IEEE Rev. Biomed. Eng.*, vol. 13, pp. 32–50, 2020.

[11] Y. Zhao et al., "Remote vascular interventional surgery robotics: A literature review," *Quantitative Imag. Med. Surg.*, vol. 12, no. 4, pp. 2552–2574, 2022.

[12] M. E. M. K. Abdelaziz, L. Tian, M. Hamady, G.-Z. Yang, and B. Temelkuran, "X-ray to MR: The progress of flexible instruments for endovascular navigation," *Prog. Biomed. Eng.*, vol. 3, no. 3, 2021, Art. no. 032004.

[13] I. Rykowska, I. Nowak, and R. Nowak, "Drug-eluting stents and balloons, structure designs, and coating techniques: A review," *Molecules*, vol. 25, no. 20, 2020, Art. no. 4624.

[14] K. Morino, S. Kikuchi, S. Chikagawa, M. Izumi, and T. Watanabe, "Sheet-based gripper featuring passive pull-in functionality for bin picking and for picking up thin flexible objects," *IEEE Robot. Automat. Lett.*, vol. 5, no. 2, pp. 2007–2014, Apr. 2020.

[15] S. Zhang et al., "Hardware technology of vision-based tactile sensor: A review," *IEEE Sensors J.*, vol. 22, no. 22, pp. 21410–21427, Nov. 2022.

[16] Y. She, S. Wang, S. Dong, N. Sunil, A. Rodriguez, and E. Adelson, "Cable manipulation with a tactile-reactive gripper," *Int. J. Robot. Res.*, vol. 40, no. 12–14, pp. 1385–1401, 2021.

[17] H. Rafii-Tari et al., "Objective assessment of endovascular navigation skills with force sensing," *Ann. Biomed. Eng.*, vol. 45, no. 5, pp. 1315–1327, May 2017.

[18] H. B. Khaniki, M. H. Ghayesh, R. Chin, and M. Amabili, "A review on the nonlinear dynamics of hyperelastic structures," *Nonlinear Dyn.*, vol. 110, no. 2, pp. 963–994, Oct. 2022.

[19] Y. Noh et al., "Image-based optical miniaturized three-axis force sensor for cardiac catheterization," *IEEE Sensors J.*, vol. 16, no. 22, pp. 7924–7932, Nov. 2016.

[20] Y. Zhao et al., "Surgical GAN: Towards real-time path planning for passive flexible tools in endovascular surgeries," *Neurocomputing*, vol. 500, pp. 567–580, 2022.